This PDF file includes:

Appendix Fig S1

Appendix Fig S2

Appendix Fig S3

Appendix Fig S4

Appendix Fig S5

Appendix Fig S6

Appendix Table S1-4

Appendix Figure 1

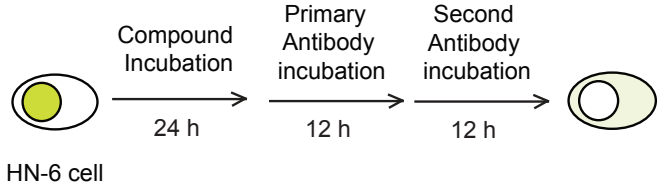

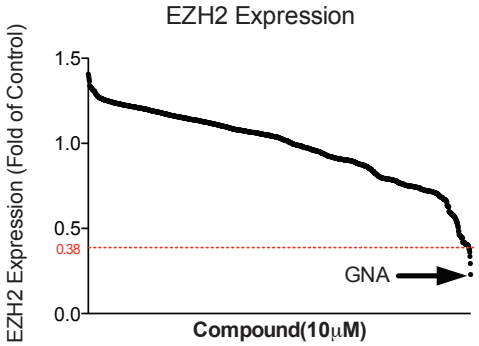

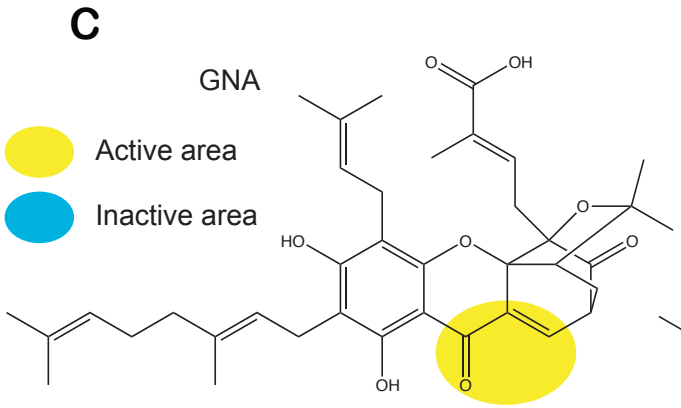

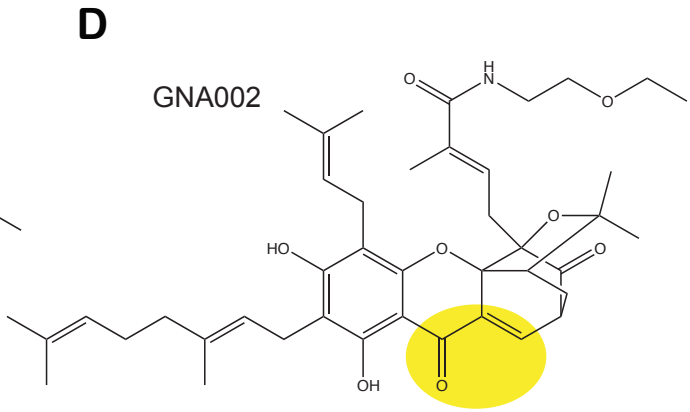

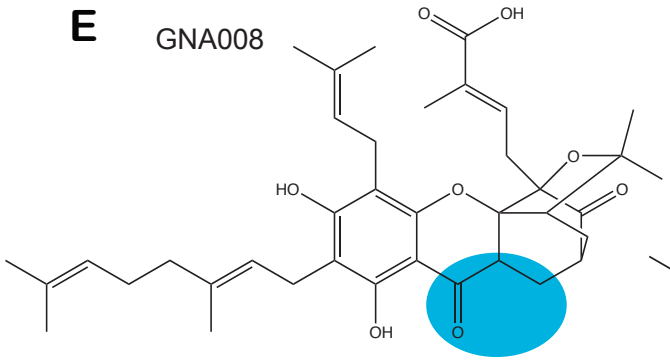

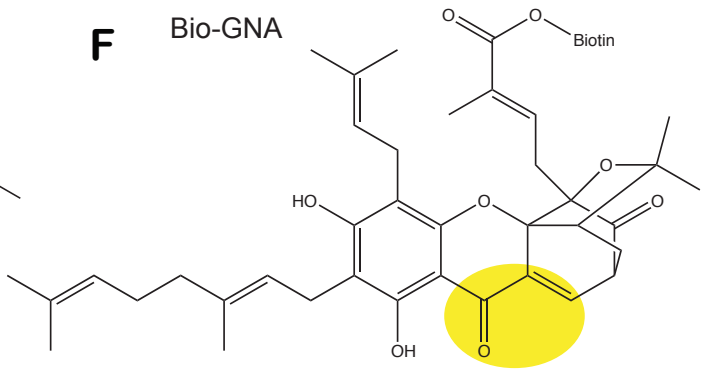

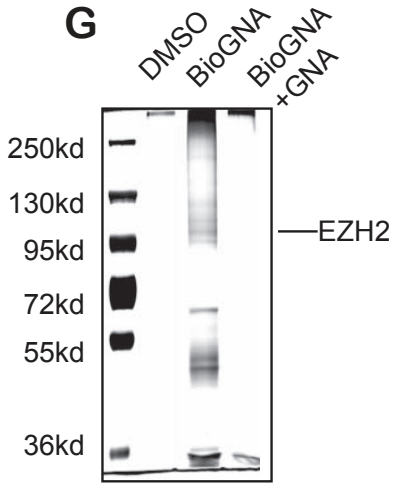

H

1	MGQTGKKSEK	GPVCWRKRVK	SEYMRLRQLK	RFRRADEVKS	MFSSNRQKIL	ERTEILNQEW	KQRRIQPVHI	LTSVSSLRGT	80
81	RECSVTSDLD	FPTQVIPLKT	LNAVASVPIM	YSWSPLQQNF	MVEDETVLHN	IPYMGDEVLD	QDGTFIEELI	KNYDGKVHGD	160
161	RECGFINDEI	FVELVNALGQ	YNDDDDDDDG	DDPEEREEKQ	KDLEDHRDDK	ESRPPRKFPS	DKIFEAISSM	FPDKGTAEEL	240
241	KEKYKELTEQ	QLPGALPPEC	TPNIDGPNAK	SVQREQSLHS	FHTLFCRRCF	KYDCFLHPFH	ATPNTYKRKN	TETALDNKPC	320
321	GPQCYQHLEG	AKEFAAALTA	ERIKTPPKRP	GGRRRGRLPN	NSSRPSTPTI	NVLESKDTDS	DREAGTETGG	ENNDKEEEEK	400
401	KDETSSSSEA	NSRCQTPIKM	KPNIEPPENV	EWSGAEASMF	RVLIGTYYDN	FCAIARLIGT	KTCRQVYEFR	VKESSIIAPA	480
481	PAEDVDTPPR	KKKRKHRLWA	AHCRKIQLKK	DGSSNHVYNY	QPCDHPRQPC	DSSCPCVIAQ	NFCEKFCQCS	SECQNRFPGC	560
561	RCKAQCNTKQ	CPCYLAVREC	DPDLCLTCGA	ADHWDSKNVS	CKNCSIQRGS	KKHLLLAPSD	VAGWGIFIKD	PVQKNEFISE	640
641	YCGEIISQDE	ADRRGKVYDK	YMCSFLFNLN	NDFVVDATRK	GNKIRFANHS	VNPNCYAKVM	MVNGDHRIGI	FAKRAIQTGE	720
721	ELFFDYRYSQ	ADALKYVGIE	REMEIP						746

The matched peptides cover **86%** (645/746 AA's) of the protein.

Protein Name: **Enhancer of zeste homolog 2 - Homo sapiens (Human)**
Species: **HUMAN**
SwissProt.human Accession #: **Q15910**
MS Digest Index #: **5244**
Masses are:
pI of Protein: **6.65**
Protein MW: **85363.7** Da
Amino Acid Composition: **A41 C34 D53 E62 F31 G38 H17 I37 K60 L42 M13 N39 P46 Q33 R52 S50 T34 V35 W7 Y22**

MS Digest - Agilent Spectrum Mill Rev. 3.3.084

Appendix Figure S1. Screening and identification of gambogenic acid (GNA) to directly interact with EZH2.

A. Scheme for screening EZH2 inhibitors from a chemical compound library.

B. Screening data for EZH2-immunoreactive signals in HN-6 nuclei. A threshold of 0.38 relative to the original EZH2 protein abundance was set to identify the top hit candidates for further validation.

C. The parental compound, GNA; the bio-active area is highlighted yellow.

D. The active derivative compound GNA002; the bio-active area is highlighted yellow.

E. The inactive derivative compound GNA008; the bio-inactive area is highlighted purple.

F. The biotin-tagged GNA derivative Bio-GNA.

G. Silver staining for Bio-GNA pull-down assays to indicate the GNA-binding proteins. Nuclear lysates derived from the HN12 head and neck cancer cells were incubated with DMSO or 10 μM Bio-GNA before the pull-down analysis. Free GNA (50 μM; non-biotin-conjugated) could efficiently compete with Bio-GNA binding with the various pull-down proteins.

H. Peptide sequences of EZH2 were identified as one of the Bio-GNA-pulled proteins by the HPLC-MS-MS analysis.

Appendix Figure 2

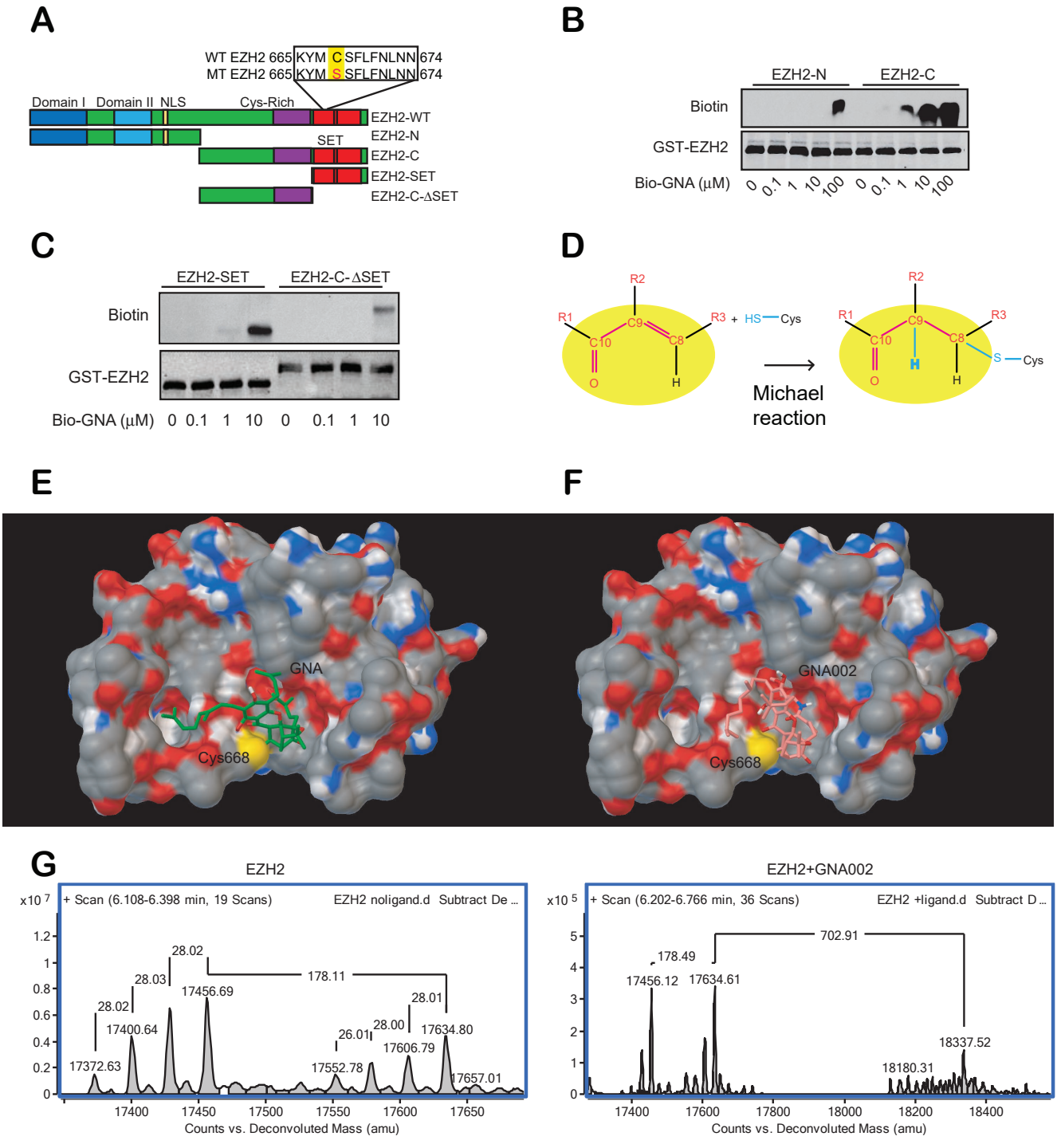

Appendix Figure S2. GNA derivative, GNA002 specifically disassociates the PRC2 complex and reduces wild type EZH2 in different cancer cell lines.

A. To determine the potential GNA binding site(s) within the EZH2 protein, GST-tagged recombinant EZH2 segments were bacterially generated and purified.

B. SDS-PAGE followed by immunoblotting analysis demonstrated that biotin signal, derived from the Bio-GNA compound, was enriched in associating with C-terminal segment, but not the N-terminal segment of EZH2 when incubated with up to 10 μM Bio-GNA for 2 hours before the biotin signal being detected with the streptavidin-HRP.

C. SDS-PAGE followed by immunoblotting analysis demonstrated that biotin signal, derived from the Bio-GNA compound, was reduced upon deletion of the Set domain in the C-terminal segment of EZH2 when incubated with up to 10 μM Bio-GNA for 2 hours before the biotin signal being detected with the streptavidin-HRP.

D. A schematic illustration of the "Michael reaction", typically formed between the C atom of a given drug with the S atom of the cysteine residue in the drug target protein.

E. A computational modeling scheme to illustrate that the C8 atom of the GNA compound could establish a favorable C-S covalent bond with the S atom in the Cys668 residue within the SET domain of EZH2..

F. A computational modeling scheme to illustrate that the C8 equivalent atom of the more active form of GNA derivative, the GNA002 compound could establish a favorable C-S covalent bond with the S atom in the Cys668 residue within the SET domain of EZH2.

G. The LC-MS analysis to detect the interaction between the EZH2 SET domain and GNA002.

Appendix Figure 3

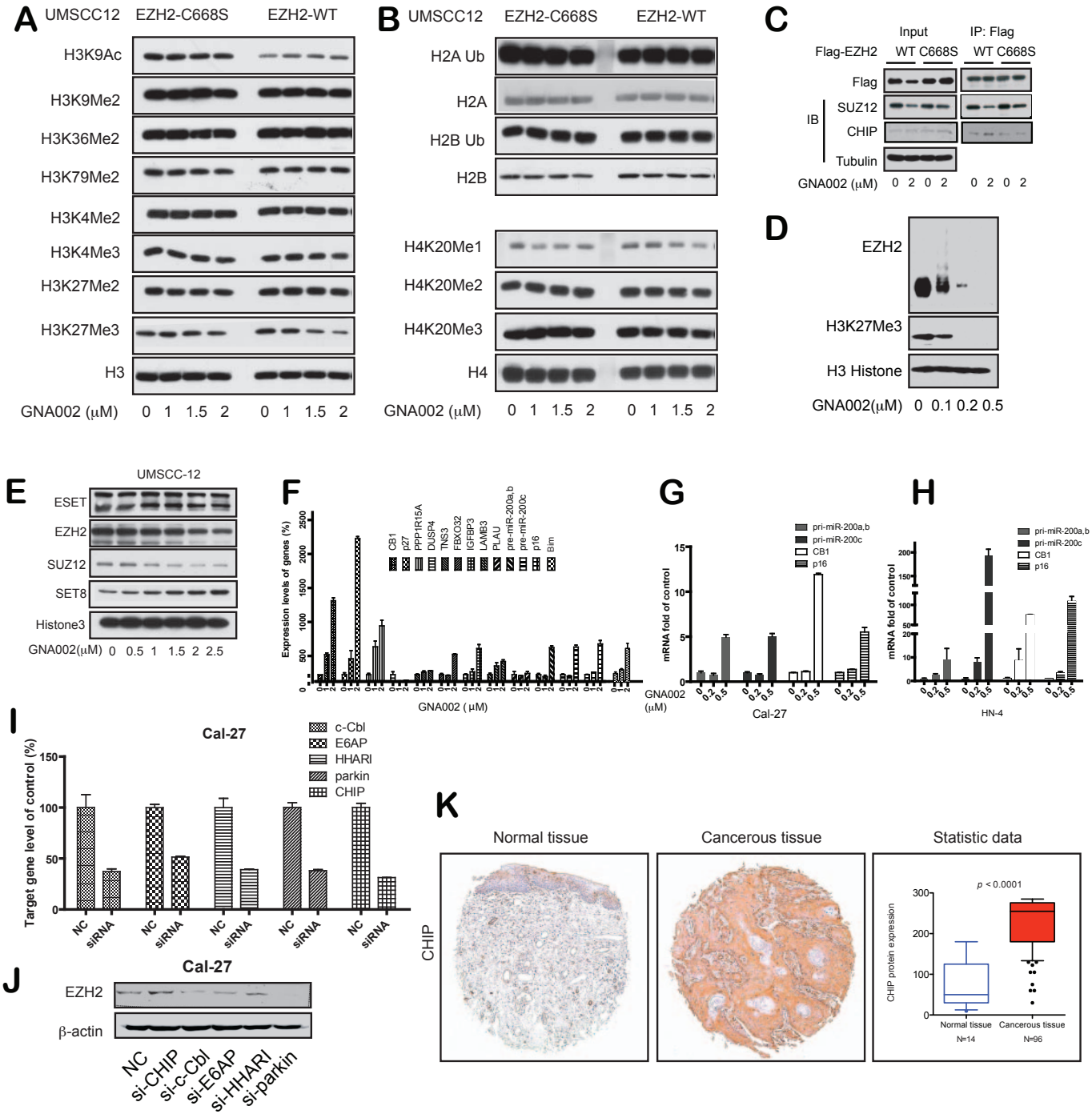

Appendix Figure S3. GNA002 specifically disassociates the PRC2 complex and reduces the abundance of wild type EZH2 in different cancer cell lines.

A. Immunoblot analysis indicated the acylation and methylation at different lysine residues of Histone 3 protein following GNA002 incubation in UMSCC-12 head and neck cancer cells ectopically expressing wild type or the C668S-mutant form of EZH2.

B. Immunoblot analysis indicated the ubiquitination of Histone 2A and 2B protein, as well as the methylation at the lysine 20 residue of Histone 4 protein following GNA002 incubation in UMSCC-12 head and neck cancer cells ectopically expressing wild type or the C668S-mutant form of EZH2.

C. Immunoblot analysis illustrated the GNA002 treatment only reduced the protein abundance of the PRC2 complex components, while the expression levels of other histone methyltransferases were not influenced.

D. Immunoblot analysis demonstrated that long-term treatment with GNA002 significantly reduced the protein abundance of endogenous EZH2 and H3K27Me3 levels in RS411 leukemia cells.

E. GNA002 treatment for 24 hours increased mRNA levels of various characterized PRC2 target genes in HN-12 head and neck cancer cells. However, the non-EZH2 targeted genes such as DUSP4, TNS3 and PLAU, were not significantly up-regulated, indicating the specificity of GNA002 in inhibiting EZH2.

F-H. Inhibition of EZH2 by GNA002 also increased the mRNA levels of various reported PRC2 target genes in epithelial head and neck cancer cell line HN-12 cells (**F**), Cal-27 cells (**G**) and HN-4 cells (**H**). Cells were treated with 0.2 μM and 0.5 μM GNA002 for 24 hours. The real-time PCR assays were performed to detect the mRNA levels.

I-J. Cal-27 head and neck cancer cells were transfected with 50 nM non-specific siRNA (negative control, NC) or specific siRNA for five genes encoding various E3 ligases including c-Cbl, E6AP, HHAR1, Parkin and CHIP, respectively. At 48 hours post-transfection, the efficiency of knockdown (KD efficiency) was determined by RT-PCR in **I**, and the changes of EZH2 protein abundance were monitored by immunoblot analysis in **J**.

K. Immunohistochemistry assays to demonstrate CHIP expression in the head and neck squamous cell carcinoma tissues was significantly higher than those in the normal epithelial tissues.

Appendix Figure 4

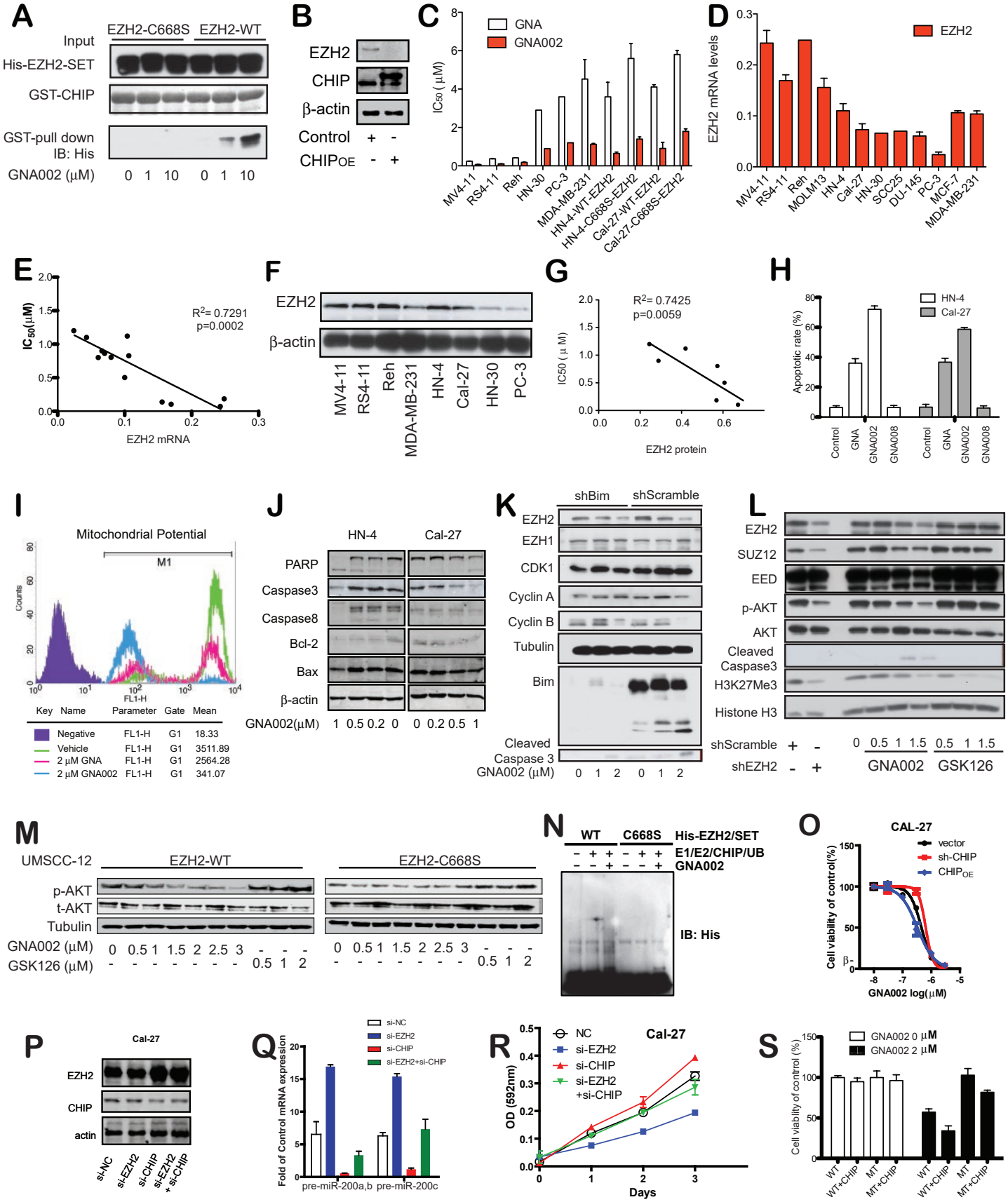

Appendix Figure S4. GNA002 and HSP90 inhibitor synergistically reduce EZH2 abundance

A. GST-pull down assays to monitor the binding changes between EZH2 SET domain and CHIP protein in the presence or absence of GNA002 incubation for 12 hours.

B. Immunoblot analysis demonstrated that ectopic expression of CHIP ($CHIP_{OE}$), conversely, reduced endogenous EZH2 levels in Cal-27 head and neck cancer cells.

C. GNA002 inhibited cell proliferation more potently than GNA. Different cell lines were incubated with GNA or GNA002 for 72 hours, followed by the MTT analyses to calculate out its IC_{50} value.

D. EZH2 mRNA levels in different cell lines were examined through real-time RT-PCR assays.

E. There is an inverse correlation between IC_{50} value of GNA002 and EZH2 mRNA levels among different cell lines we examined.

F. EZH2 protein levels in different cell lines were examined by immunoblotting assays.

G. There is an inverse correlation between IC_{50} value of GNA002 and EZH2 protein levels among different cell lines we examined.

H. GNA and an active derivative, GNA002, but not an inactive derivative, GNA008, induced cellular apoptosis. HN-4 and Cal-27 head and neck cancer cells were treated with indicated concentrations of compounds for 24 hours, followed with the PI-Annexin V-staining and FACS analysis to monitor the apoptotic status.

I. FACS analysis revealed that GNA002 was more potent than GNA to decrease cellular mitochondrial potential. Cal-27 head and neck cancer cells were treated with 2 μM GNA or GNA002 for 24 hours, followed by rhodamine123 staining and FACS analysis.

J. Immunoblot analysis to detect the induction of apoptosis-associated markers in HN-4 and Cal-27 head and neck cancer cells after being treated with the indicated concentration of GNA002 for 24 hours.

K. UMSCC-12 head and neck cancer cells were infected with lentiviral shScramble (as a negative control) and shBim constructs followed by selection with 1 μg/ml puromycin for 72 hours to eliminate the non-infected cells. Afterwards, the resulting cell lines were treated with varied concentrations of GNA002 for 24 hours before collecting whole cell lysates for immunoblots with the indicated antibodies.

L. Immunoblotting assays indicated that both shEZH2 and GNA002 treatment decreased EZH2 protein and H3K27Me3 levels and induced Caspase 3 cleavage, while the methyltransferase inhibitor, GSK126, only reduced H3K27Me3 levels in UMSCC-12 cells.

M. Immunoblotting assays demonstrated that GNA002 could inhibit AKT phosphorylation only in the wild type of EZH2-expressing UMSCC-12 cells, but not in the C668S-mutant expressing cells.

N. *In vitro* ubiquitination assays showed that CHIP only increased the ubiquitination levels of WT-EZH2-SET protein in the presence of GNA002.

O. The IC_{50} values, indicating cellular sensitivity to GNA002 incubation for 72 hours, were plotted for Cal-27 cells either depleted of endogenous CHIP, or ectopically expressing WT-CHIP (empty vector was used as a negative control).

P. Cal-27 cells were transfected with 50 nM of different siRNAs, including non-specific siRNA (NC), specific siRNA to EZH2, specific siRNA to CHIP or pool siRNA of EZH2 and CHIP, respectively. At 48 hours post-transfection, the efficiency of knockdown and the expression changes of EZH2 were determined by immunoblot analysis.

Q. RT-PCR analysis revealed that GNA002 treatment showed synergistic effects with depletion of endogenous EZH2 by si-EZH2 RNAs on inducing mRNA expression of EZH2-targeted genes. However, depletion of endogenous CHIP by si-CHIP RNAs could partially block GNA002-induced reactivation of EZH2 targets.

R. The cell proliferation after each siRNA transfection as described in **Q** was examined using MTT assays at the indicated time points.

S. Ectopic expression of CHIP conferred UMSCC12 cells expressing wild type EZH2 (WT), but not the non-GNA002-interacting, C668S-mutant form of EZH2 (MT), more sensitive to GNA002-mediated growth inhibition.

Appendix Figure 5

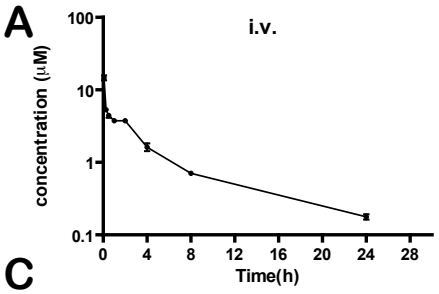

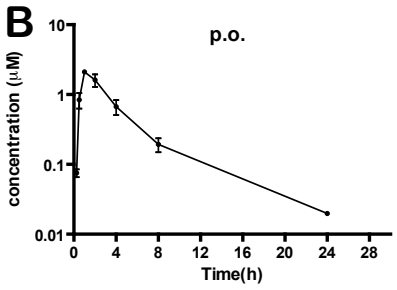

C

	$AUC_{(0-t)}$	$AUC_{(0-\infty)}$	$MRT_{(0-\infty)}$	$t_{1/2z}$	T_{max}	Vz	CLz	C_{max}	F
	μM*hr	μM*hr	hr	hr	hr	L/kg	L/hr/kg	μM	%
IV (12 mg/kg)	27.4	29.11	6.28	6.68	0.08	5.66	0.59	14.69	NA
PO (12 mg/kg)	8.44	8.56	4.38	4.16	1	NA	NA	2.11	29.4

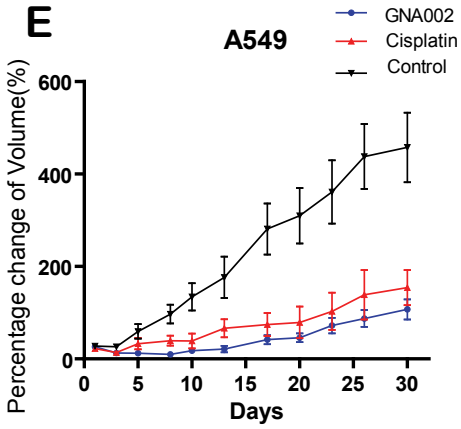

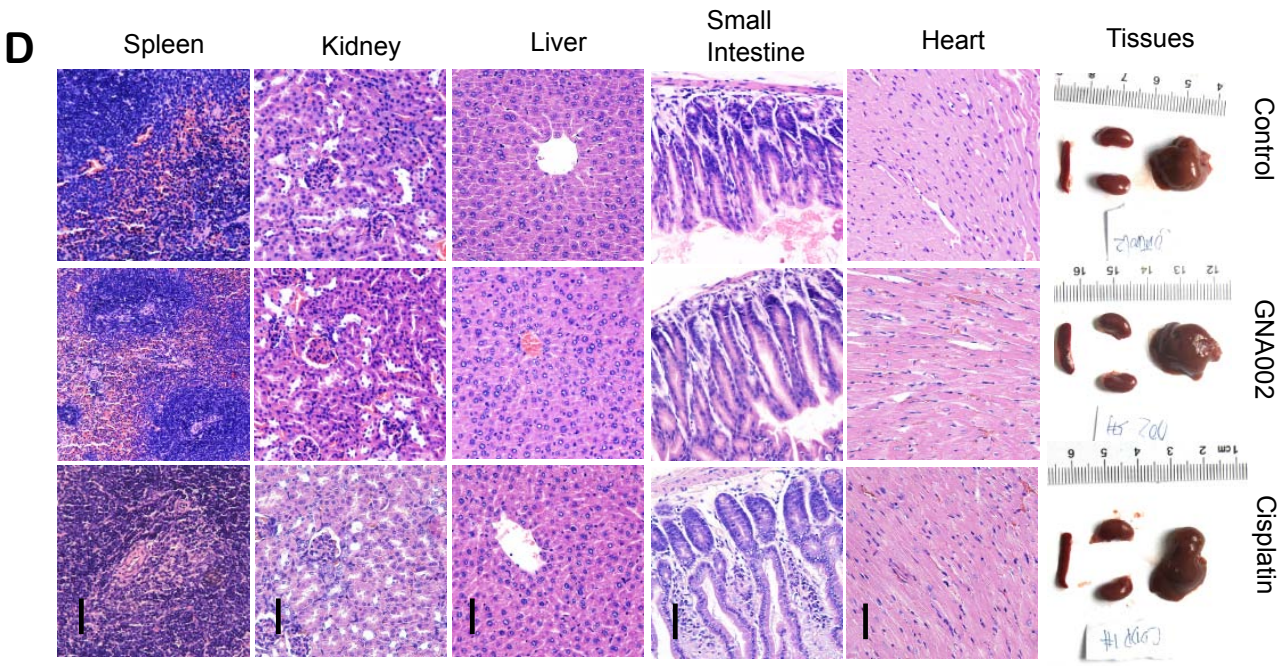

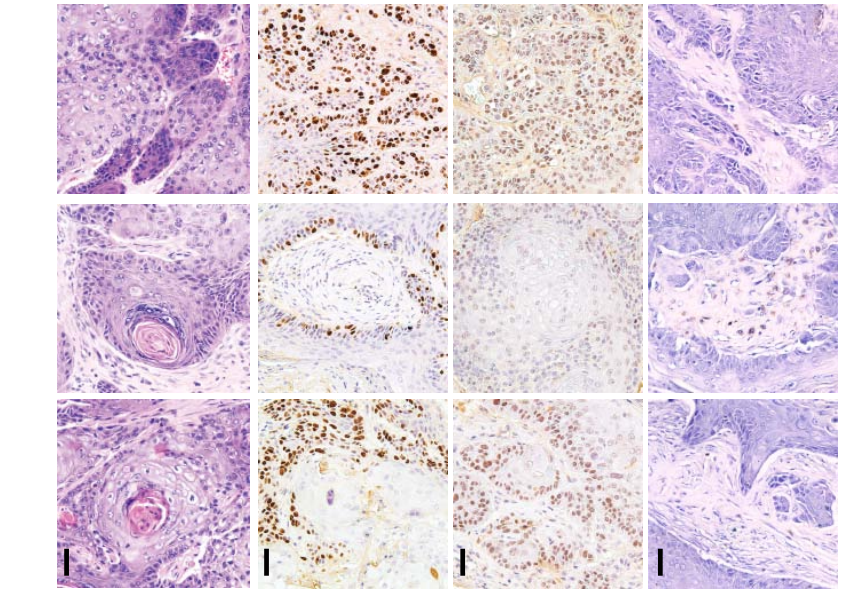

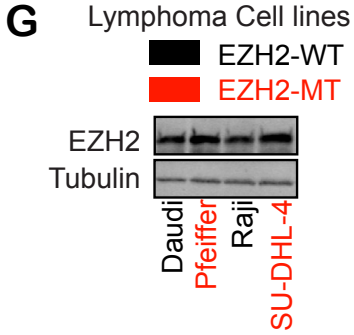

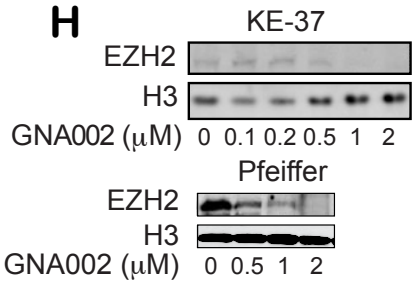

Appendix Figure S5. GNA002 significantly inhibits tumor growth largely through promoting the ubiqutination and subsequent degradation of EZH2.

A. Graphical representations of GNA002 levels in plasma samples collected from ICR mice up to 24 hours post-single dosing of 12 mg/kg by injection via veins. The values are presented as the mean ± SD, n=10.

B. Graphical representations of concentration of oral gavage GNA002 levels. The values are presented as the mean ± SD, n=10.

C. Illustration of the pharmacokinetics of the GNA002 compound in ICR mice.

D. H&E staining demonstrated that unlike the non-specific toxicity of the chemotherapeutic agent, cisplatin, GNA002 did not exert a significant toxic effect on various tissues derived from the xenografted nude mice. Bar, 300 μm.

E. Oral treatment of GNA002 inhibited the *in vivo* tumor growth of the lung cancer cell line A549.

F. Tissues derived from epithelial head and neck Cal-27 cancer cell xenografted tumors were harvested from mice treated with vehicle, GNA002 and cisplatin, respectively. The morphological changes were examined by H&E staining, and cell proliferation was examined by IHC staining for EZH2 and Ki67. The apoptotic cells were identified by TUNEL assays. Bar, 200 μm.

G. Immunoblotting assays indicated EZH2 expression in wild type (WT, such as Daudi and Raji cell lines) and mutant (MT, such as Pfeiffer and SU-DHL-4 cell lines) EZH2-expressing lymphoma cells

H. Immunoblotting assays demonstrated that GNA002 treatment could lead to comparable reduction of EZH2 protein abundance in KE-37 T-ALL cells whose growth is not dependent on EZH2 enzymatic activity, as well as the Pfeiffer lymphoma cell line that is addicted to the onogenic function of EZH2.

Appendix Figure 6

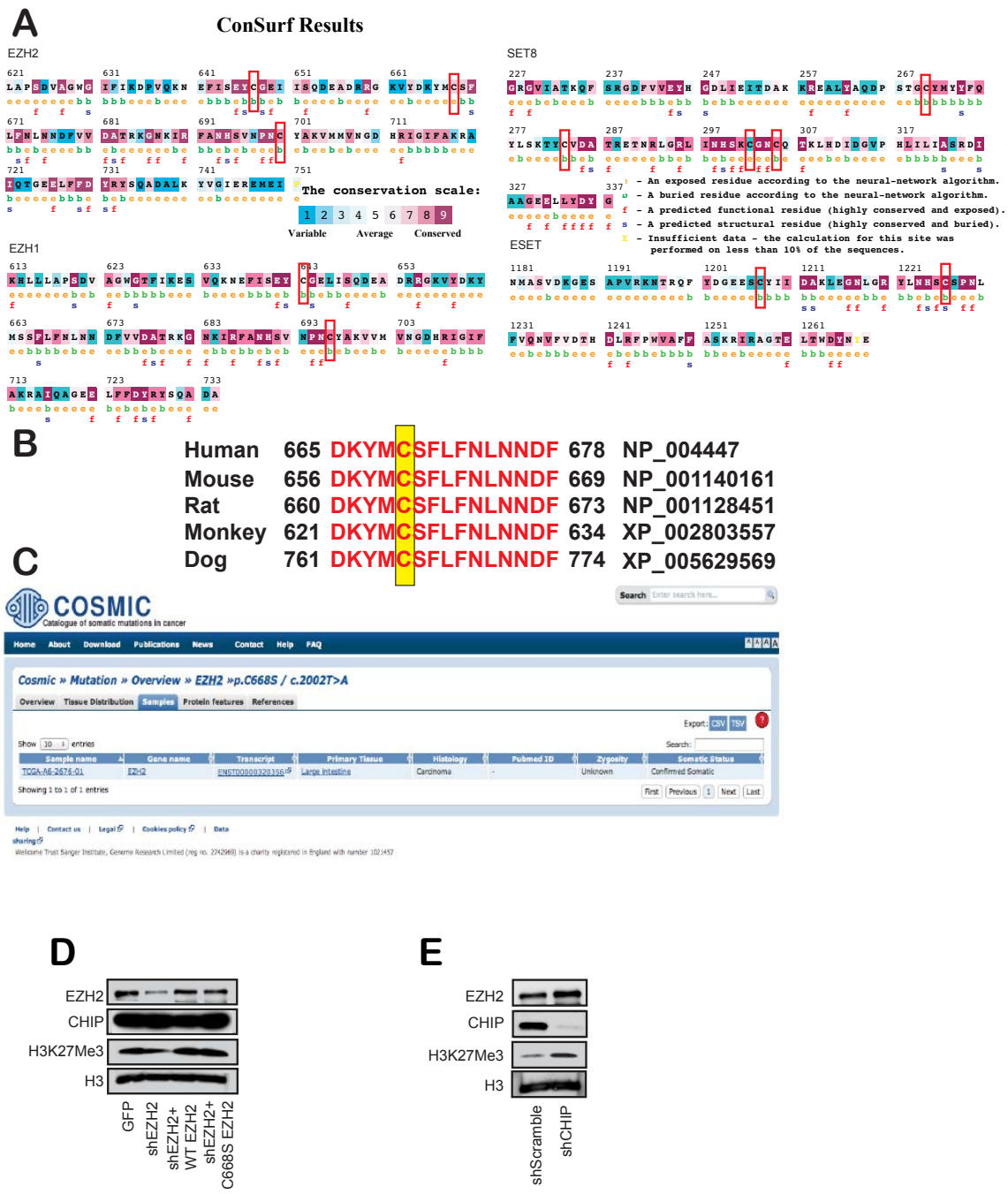

Appendix Figure S6. GNA002 significantly inhibits tumor growth through CHIP-medidated degradation of the covalently bound EZH2 oncoprotein.

A. Bioinformatic analysis with the software from the ConSurf website to evaluate the distribution of cysteine residues in different histone methyltransferases revealed that only EZH2 contained a cysteine residue (Cys668) on the protein surface and is available for the Michael reaction.

B. A schematic illustration showed that the Cys668 residue, which is highlighted in yellow, is evolutionarily conserved.

C. The sporadic C668S mutation has been discovered in the colon cancer samples on the COSMIC website.

D. UMSCC-12 head and neck cancer cells were infected with lentiviral shEZH2 constructs (with shGFP as a negative control) to deplete endogenous *EZH2*, which led to a significant reduction in H3K27-trimethylation. The EZH2-depleted UMSCC12 cells were then infected with lentivirus encoding either WT-EZH2, or the non-GNA-interacing C668S mutant form of EZH2. Afterwards, the EZH2 and H3K27me3 levels were examined with immunoblot analysis on whole cell lysates derived from these generated cell lines.

E. UMSCC-12 cells were infected with lentiviral shCHIP constructs (with shGFP as a negative control) to deplete endogenous *CHIP*. The EZH2 and H3K27me3 levels were examined with immunoblot analysis on whole cell lysates derived from these generated cell lines.

Appendix Tables

Appendix Table S1. The list of GNA-associating Proteins identified with LC/MS/MS

Protein Name	Distinct Peptides	% AA Coverage
Heat shock protein HSP 90-beta	10	18
Tubulin beta-2B chain - Homo sapiens (Human)	9	32
Enhancer of zeste homolog 2 - Homo sapiens (Human)	8	18
Heat shock protein HSP 90-alpha 2	5	8
Splice Isoform 1 of Interleukin enhancer-binding factor 3	4	6
Splice Isoform Long of Delta 1-pyrroline-5-carboxylate synthetase	4	7
Interleukin enhancer binding factor 3 isoform c variant	3	9
DEAH (Asp-Glu-Ala-His) box polypeptide 15	3	4
Putative pre-mRNA splicing factor RNA helicase	3	4
HNRPR protein	3	6
Cytokeratin type II	2	4
DEAD-box protein 50	2	4
Splice Isoform 1 of DNA replication licensing factor MCM7	2	4
MinichroMosoMe Maintenance protein 7 isoforM 2	2	6
Nucleolar RNA helicase II	2	2
DEAD\/H (Asp-Glu-Ala-Asp\/His) box polypeptide 21	2	2
Hypothetical protein DKFZp686F21172	2	3

Appendix Table S2. The EZH2 inhibitbory effects of various GNA derivatives

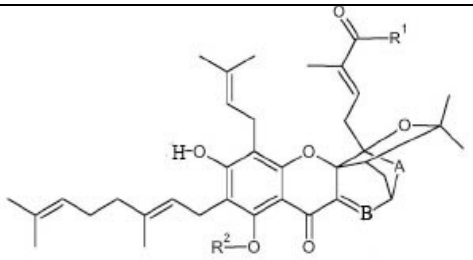

Compounds	R^1	R^2	A	B	EZH2 inhibition IC_{50} (μM)
GNA	-OH	-H	-CO-	-CH-	8.6
GNA001	$-OCH_2$	-H	-CO-	-CH-	2
GNA002	$-NHCH_2CH_2OCH_2CH_3$	-H	-CO-	-CH-	1.1
GNA003	-OH	$-CH_2CH_3$	-CO-	-CH-	9.6
GNA004	-OH	-H	-COH-	-CH-	>20
GNA005	$-N(CH_2CH_3)_2$	-H	-CO-	-CH-	3.5
GNA006	$-N(CH_2CH_2)_2NCOCH_3$	-H	-CO-	-CH-	2.1
GNA007	$-N(CH_2)_5$	-H	-CO-	-CH-	5.1
GNA008	-OH	-H	-CO-	$-CH_2-$	>20
Bio-GNA	-O-biotin	-H	-CO-	-CH-	10.5

Appendix Table S3. IC_{50} values of GNA derivatives in different cell lines.

	GNA IC_{50}±SD (μM)	GNA002 IC_{50}±SD (μM)
HN-4	3.129±0.543	0.502±0.082
HN-6	3.522±0.432	0.783±0.112
HN-12	4.121±0.265	0.818±0.123
HN-13	2.942±0.177	0.782±0.083
Cal-27	4.241±0.247	0.804±0.191
SCC-25	3.761±0.453	0.862±0.078
HeLa	5.411±0.924	1.486±0.133
SMMC-7721	5.751±0.896	1.670±0.274
MCF-7	2.876±0.312	0.827±0.111
MCF-7/ADM	4.926±0.869	1.110±0.211
KB	3.111±0.232	1.410±0.181
KB/VCR	5.177±0.962	1.588±0.211
MDA-MB-231	4.524±1.010	1.121±0.052
MDA-MB-468	2.577±0.847	0.732±0.117
A549	4.577±1.311	1.212±0.231
HT-29	3.121±0.782	0.917±0.162
HL-60	1.868±0.481	0.577±0.081
SGC-7901	4.647±0.693	0.786±0.214
MV4-11	0.246±0.005	0.070±0.003
RS4-11	0.373±0.005	0.103±0.007
Reh	0.420±0.004	0.184±0.013
Daudi	0.542±0.085	0.059±0.007
Pfeiffer	0.383±0.075	0.024±0.002
KE-37	3.433±0.064	1.222±0.068

Appendix Table S4. The growth inhibitory effects of different GNA derivatives in Cal-27 head and cancer cells.

	100 μM	10 μM	1 μM	0.1 μM	0.01 μM	Effect
GNA	100%	100%	5%	0	0	+
GNA002	100%	100%	98%	12%	0	++
GNA008	50%	0	0	0	0	-
Bio-GNA	100%	87%	57%	0	0	+

A value of 100% indicates a total blockage of cell growth *in vitro* as detected by MTT assays, while less significant growth inhibitory effects were observed at lower concentrations of the indicated GNA derivatives. In contrast, the biologically inactive form of GNA derivative, GNA008, exerted the lowest biological effects in suppressing Cal-27 growth even at its highest concentration.